Korean J. Chem. Eng., **28**(5), 1299-1303 (2011)
DOI: 10.1007/s11814-010-0500-4

Microwave synthesis of mesoporous WO_3 doping with bismuth and photocatalytic oxidation of water to H_2

Lixia Zou, Qingcheng Liu†, Qiong Xu, and Guanjie Mi

Key Laboratory of Radioactive Geology and Exploration Technology Fundamental Science for National Defense, East China Institute of Technology, Fuzhou Jiangxi 344000, China
(*Received 16 June 2010 • accepted 1 December 2010*)

Abstract−Mesostructured tungstic acid was prepared from Na_2WO_4 with protonated cation-exchange using a surfactant cetyltrimethyl ammonium bromine (CTAB) as the structure-directing agent under microwave radiation. The surfactant was removed by high-temperature calcination, microwave radiation extraction and Soxhlet extraction, respectively. The effects of these methods for removal of the surfactant were investigated in detail. XRD, TEM, FT-IR and UV-Vis were employed to characterize the mesostructured materials. The results showed that the microwave extraction and Soxhlet extraction were favorable to the synthesis of mesostructured tungstic oxide. Mesoporous structure was destroyed as the calcining temperature rising to 823 K. The mesoporous structure of WO_3 prepared by microwave radiation extraction had an average pore diameter of 3.4 nm and specific surface area of 120.46 $m^2 \cdot g^{-1}$. And also, the mesoporous materials WO_3 doping with Bi_2O_3 displayed much higher photocatalytic activity than commercial Degussa P25 TiO_2 under visible light and UV irradiation.

Key words: Mesoporous WO_3, Microwave Radiation, Microwave Extraction, Photocatalytic Activity

INTRODUCTION

Tungsten (VI) oxide (WO_3), a material with a band gap of 2.8 eV, recently has received considerable research attention for photocatalytically oxidizing the organic pollutants and oxidizing water to generate H_2 [1,2] due to its excellent properties, such as good response capabilities in the solar spectrum, resistance to photoinduced corrosion, ease of handling and harmlessness. WO_3, however, has lower light energy conversion efficiency than the widely used TiO_2. Numerous investigations have reported that the doping of metal or metal ions could make the spectrum of WO_3 move towards the visible region, increase the light absorption ability and expand the excited range of WO_3 [3,4]. Actually, visible light-induced action of oxidizing water by WO_3 powder has been reported using iron (III) ions (or silver ions) as the electron acceptor [5,6].

Mesoporous materials with ordered pore structures and high surface areas are technologically important for a variety of applications such as in heterogeneous catalysis, adsorption, chemical sensing, electrodes, transportation/storage of fluids and gases, and also in some biological areas [7-9]. However, mesoporous tungsten oxide loaded by Bi_2O_3 particles using microwave synthesis to be used as an photocatalyst has not been reported as far. In this paper, mesoporous WO_3 had been prepared by microwave heating. The Bi^{3+} ion was chosen as an electron acceptor owing to its high stability in aqueous solutions, its excellent ability to absorb light and its highly reversible reduction on oxide surfaces [10]. This kind of mesostructured catalyst shows high photocatalytic activity for oxidation of water to H_2.

†To whom correspondence should be addressed.
E-mail: aabb-ccdd-@tom.com

EXPERIMENTAL

1. Chemicals

Cetyltrimethyl ammonium bromine (CTAB), 1-hexanol (98%, GC), butanol, $Na_2WO_4 \cdot 2H_2O$, bismuth nickel, protonated cation exchange resin and formaldehyde were G.R. grade.

2. Synthesis

2-1. Preparation of Precursor

$Na_2WO_4 \cdot 2H_2O$ aqueous solution was allowed to flow down through the glass column packed with the protonated cation exchange resin at a rate of 2 cm^3/min, and the effluent was collected in a beaker as the tungsten acid sol. Then, dissolved cetyltrimethyl ammonium bromine (CTAB) was added to the tungsten acid sol while stirring. The precursor mixture was oscillated vigorously for 20 min and aged for 24 h. All the operations above were carried out at room temperature. Then, the precursor mixture was heated for 1h in a microwave oven with a temperature-controllable program at a constant output power of 780 W.

2-2. Removal of the Surfactant Species

The products above were washed with acetone several times, and the surfactant was removed completely by extraction with boiling toluene solution under microwave radiation for 1 h or by Soxhlet extraction for 16 h. Then, the extracted samples were dried and calcined at 160 °C for a few minutes in a microwave oven, respectively. The powders prepared with microwave extraction and Soxhlet extraction were denoted as the symbol "Wm" and "Ws", respectively. The surfactant CTAB can also be removed completely with traditional calcining in muffle oven for 2 h at 550 °C. The sample prepared with traditional calcining was denoted as "Wc". The sample $WO_3 \cdot Bi_2O_3$ in the paper was prepared with the Bi_2O_3 loaded in the sample Wm with the similar process above.

3. Characterization

Low-angle X-ray diffraction (XRD) patterns were collected in θ-2θ mode using a Bruker D8 Advance X-ray diffractometer (Cu Kα_1 irradiation, λ=1.5406 Å). Wide-angle XRD patterns were collected in an X-ray diffractometer (Bruker-axs D8 Advance, Germany) using Cu Kα radiation (λ=1.545 Å), while the crystallite sizes of samples were evaluated from the full width of the half maximum intensity (FWHM) values from X-ray diffractometer (XRD) peaks according to Scherrer's equation. The morphological characteristics were characterized by transmission electron micrography (TEM) (JEOL JEM-2100, Japan). Nitrogen adsorption-desorption isothermals were obtained by using ASAP-2000 equipment (Micromeritics Company, America) (analysis gas: 99.99% nitrogen, temperature 77 K). Brunauer-Emmett-Teller (BET) surface areas were estimated over a relative pressure (P/P_0) ranging from 0.05 to 0.30. Pore size distributions were obtained using the Barret-Joyner-Halenda (BJH) model and the Horvath-Kawazoe's approach for micropore determination. The optical absorbency was analyzed based on the UV/vis diffuse reflectance spectrophotometer. The structural behavior of tungsten oxide was characterized by Fourier-transform infrared spectrophotometer (FTIR) (Nicolet magna-FTIR550, Boruo Company, America).

4. Photocatalytic Water Decomposition

The photocatalytic activity for the overall water decomposition was investigated on a series of WO_3 samples prepared in a Pyrex glass reactor. Aqueous suspensions of metal oxides were prepared by dispersing 0.8 g of the oxide samples in deionized water, followed by the addition of required amounts of Bi^{3+} aqueous solutions so that the final volume was about 450 ml. The experiments were carried out at room temperature and aqueous suspensions were irradiated by a high-pressure Hg lamp (500 W) in a setup or by the visible light which passes through to filtered out the UV of medium-pressure mercury lamp by Pyrex glass with the thickness of 0.25 inch. Before irradiation, the system was evacuated several times. Amounts of gases evolved were analyzed by a gas chromatograph directly connected to the reaction system.

RESULTS AND DISCUSSION

1. XRD and Infrared Spectra

The low angle and wide angle XRD patterns of the samples (Wm, Ws, Wc) are shown in Fig. 1 and Fig. 2, respectively. LXRD shows the intense and sharp peak for the samples Wm and Ws, which suggests a highly organized mesostructure. The calcination-treated powder (Wc), however, did not exhibit such a characteristic peak, suggesting the collapse of the mesoporous framework. In Fig. 2, the samples Wm and Wc exhibited WO_3 crystalline phase, and the diffraction peak of the former was broader than that of the latter. But the samples Ws synthesized by Soxhlet extracting presented the diffraction peak of $WO_3 \cdot 0.33H_2O$ crystalline phase. Moreover, the diffraction peak of samples Wm and Wc were more intense than that of the samples Ws, which means that the samples Wm were composed of smaller crystals; the samples Wm and Ws had higher crystallinity than the samples Wc. And it was shown that microwave heating or calcining could accelerate the dehydration and crystallization of tungstic acid and microwave heating also could control the crystallite size of the materials prepared [11-13]. The size of crystallite (d) evaluated by Scherrer's equation is also shown in Table 1.

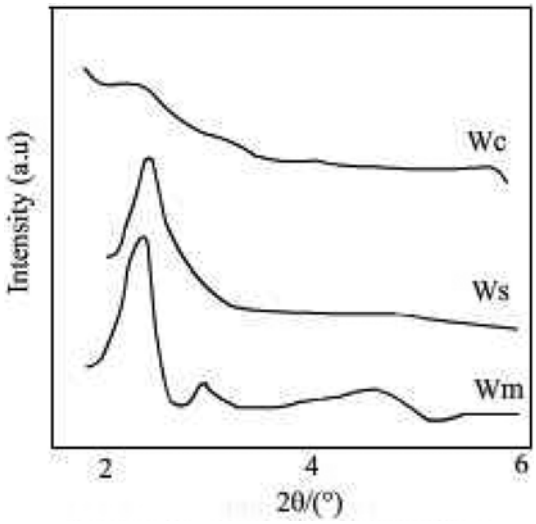

Fig. 1. Low-angle XRD patterns of samples prepared.

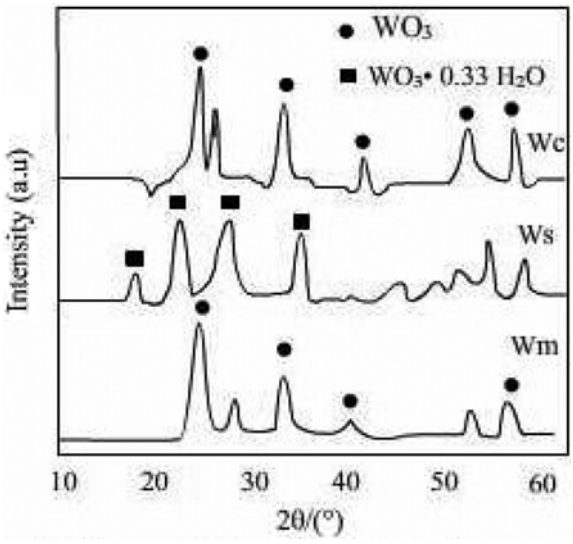

Fig. 2. Wide-angle XRD patterns of samples prepared.

Table 1. The properties of samples prepared

Sample	S_{BET}/ $m^2 \cdot g^{-1}$	D_{BJH}/ nm	V_{Pore}/ $cm^3 \cdot g^{-1}$	D/nm	Eg/ eV (λ/nm)
Wm	120.46	3.4	0.107	6.3	2.48 (500)
Ws	53.91	2.9	0.054	7.3	2.67 (465)
Wc	18.41				2.76 (450)
WO_3*	14				
$Wm \cdot Bi_2O_3$					2.88 (430)
					2.07 (600)

The infrared spectra of samples Wm prepared before and after microwave extraction were indicated in Fig. 3. As shown in Fig. 3(a), the infrared spectra of samples Wm before extracting exhibited a series of absorption bands. On one hand, the band at 3,462.44 cm^{-1} was assigned to the O-H stretching vibration, and the band at 2,947.45

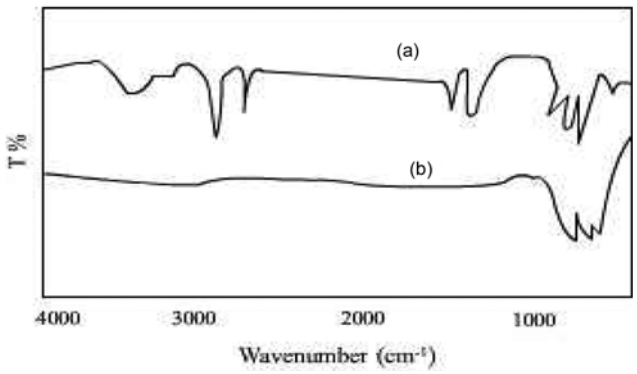

Fig. 3. FT-IR spectras of the sample. (a) Before of microwave extracting. (b) Behind of microwave extracting.

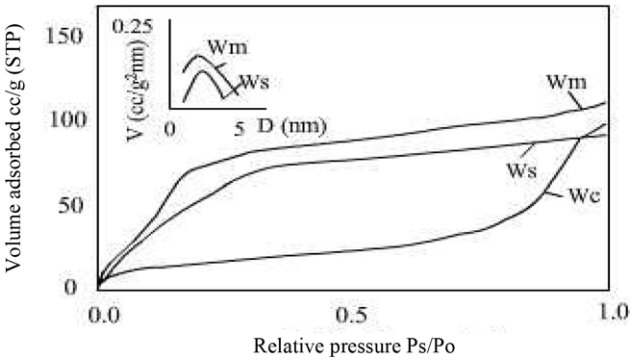

Fig. 5. Isotherms of N_2 adsorption curve for samples.

cm^{-1} was attributed to the CH_3 dissymmetry stretching vibration; the band at 2,857.86 cm^{-1} was C-H of CH_2 bond symmetry stretching vibration, and the bands at 1,456.32 cm^{-1} and 1,472.64 cm^{-1} were the CH_2 bending vibration. These were all characteristic peaks of CTAB, which suggested that some surfactant was present in the samples Wm without microwave extraction. On the other hand, the bands in the 929.2 cm^{-1}, 879.6 cm^{-1} and 773.6 cm^{-1} regions exhibited a strong absorption in Fig. 3(a), which were assigned to the Keggin framework, $W_{12}O_{40}^{8-}$ ion, demonstrating that the mesoporous WO_3 synthesized had the Keggin structure. In Fig. 3(b), Bands at 600 and 1,000 cm^{-1} were associated with the W-O-W stretching modes. Obviously, these were only characteristic peaks of tungsten oxide, for there exists terminal stretching mode band W-Od at 863.27 cm^{-1}, corner-sharing vibration band υ-W-Ob at 774 cm^{-1}, and superoxide vibration band υW-O-O-W at 544 cm^{-1} [14,15]. The surfactant CTAB, therefore, was removed completely after microwave extraction.

2. TEM and N_2-sorption Measurement

TEM morphology images of materials prepared are presented in Fig. 4. The novel findings in this work demonstrated that WO_3 prepared under different conditions exhibited different morphologies. The morphology of WO_3 prepared by calcining was regularly arranged cubic-rhombus, and the morphology of WO_3 (Wm) and $WO_3 \cdot 0.33H_2O$ (Ws) prepared by microwave-heating, were nano-particles. The crystallite sizes were smaller and had a worm hole-like mesoporous structure, which was in excellent accordance with the XRD results above. The temperature increase within the particles could have an important effect on the dynamics of particle growth. Rapid volumetric heating by microwave and differences of absorb ability of surfactants and the growing crystal faces may result in intricate and variable crystal morphologies [16].

The N_2 isotherm adsorption data and BJH size distribution of materials synthesized above are displayed in Fig. 5. The isotherm curves of the materials prepared by microwave extraction were similar to that of the materials prepared by Soxhlet extraction. Two isotherms had in common the feature that corresponds to type IV, which was typical for mesoporous materials like zeolites. Compared with the former two samples, however, the N_2-sorption isotherms of the samples Wc showed a decrease in volume adsorbed at low pressure, which was associated to some loss of mesoporous structure in the framework. The specific surface area data evaluated from these isotherms are shown in Table 1. The microwave extraction samples (Wm) had the highest specific surface areas of 120.46 m^2/g, and Soxhlet-extraction samples (Ws) was 55.91 $m^2 \cdot g^{-1}$. But the specific surface areas and pore volumes of calcining samples (Wc) were only 24.52 $m^2 \cdot g^{-1}$ and 0.049 $cm^3 \cdot g^{-1}$, respectively, and the reason is that sintering could destroy the mesostructure and the pore size distribution. The fact that the samples exhibited such high specific surface area and large pore volume was partially due to the mesoporous structure of zeolite-like and the uniform pore distribution, Moreover, compared with Soxhlet extraction and traditional calcining, microwave heating extraction aids to prevent crystals from aggregating and to reduce the crystal size. The specific surface area of the samples Wm was about 9 times as large as that of nanocrystalline WO_3 synthesized by hydrothermal method reported by Mr.

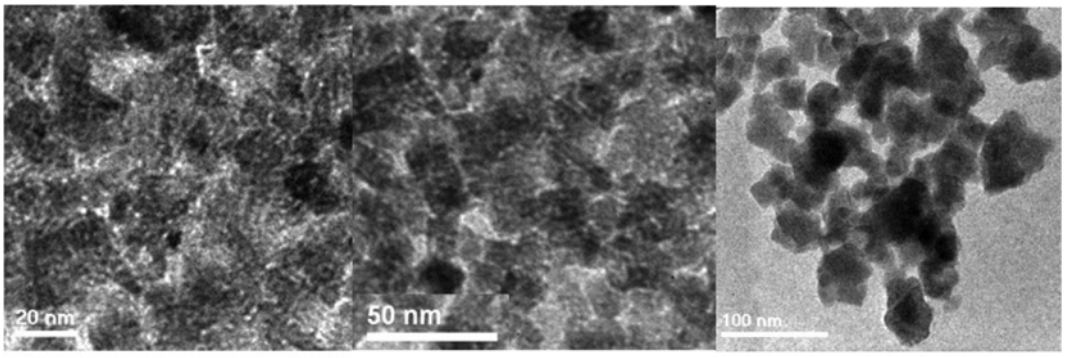

Fig. 4. TEM image of the samples.

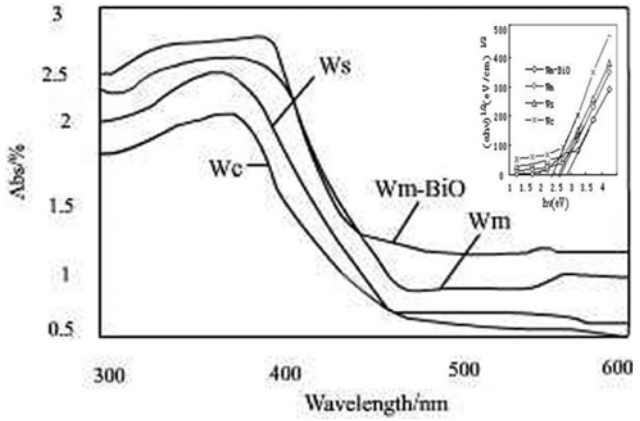

Fig. 6. UV/vis absorption spectra of the the materials synthesized. The inset is plots of $(ah\upsilon)^{1/2}$ versus photon energy, where a is the absorption coefficient.

H. K. [4].

The analysis above showed that the removal of the surfactant species gives a hollow mesoporous structure by using extraction. Calcination of the mesostructured material could have led to partial collapse of pores, which was responsible for the decrease of specific surface area. The products synthesized by microwave extraction had a larger, more regular and uniform mesoporous structure than those synthesized by conventional extraction, which suggests that the surfactant and microwave heating may be necessary for the formation of uniform mesoporous structured materials.

3. UV-vis Spectrum

Fig. 6 shows the UV/visible spectra of the materials synthesized. All four samples have high optical absorption over the whole UV-light region. The fast decay below 380-440 nm is due to the absorption of light caused by the excitation of electrons from the valence band to the conduction band of WO_3. It is worth mentioning that the absorption edge wavelength of mesoporous WO_3 shows a gradual pseudo-"red shift" with increasing the specific surface area.

The band gap energies (Eg) estimated from the $(ah\upsilon)^{1/2}$ versus photon energy plots are 2.76, 2.67 and 2.48 eV for the Wc ,Ws and Wm, respectively (Table 1). For mesoporous $Wm{\cdot}Bi_2O_3$ displayed two optical absorption thresholds at 430 nm and 600 nm that corresponded to the band gap energies of 2.88 and 2.07 eV, respectively. The solar wavelength spectrum measured here had maximum luminescence in the wavelength region of 450-480 nm. Since $Wm{\cdot}Bi_2O_3$ ($WO_3{\cdot}Bi_2O_3$), whose band gap corresponds to this region, could absorb relatively higher photon flux compared with commercial WO_3 or other samples above, it was likely to exhibit photocatalytic activity in visible light region [7,17,18].

4. Photocatalytic Decomposition of Water

The Bi_2O_3 loading on the mesoporous WO_3 was found to be especially beneficial for the overall water decomposition in UV and visible light region. The amount of Bi_2O_3 loading was then optimized and results are listed in Table 2. The samples loading of less than 2.0 wt% Bi_2O_3 did not lead to stoichiometric gas evolution and exhibited the same photocatalytic activity with Wm. The results showed that 7.0 wt% Bi_2O_3 loading was found to be the optimum amount.

As shown in Fig. 7, the comparison between the photocatalytic activity for water decomposition over samples Wm, Ws, $Wm{\cdot}Bi_2O_3$

Table 2. Optimization of the amount of BiO loading

Amount of BiO/(wt%)	2.0	4.0	7.0	9.0
H_2 evolution/$\mu mol{\cdot}h^{-1}$	59	112	167	138

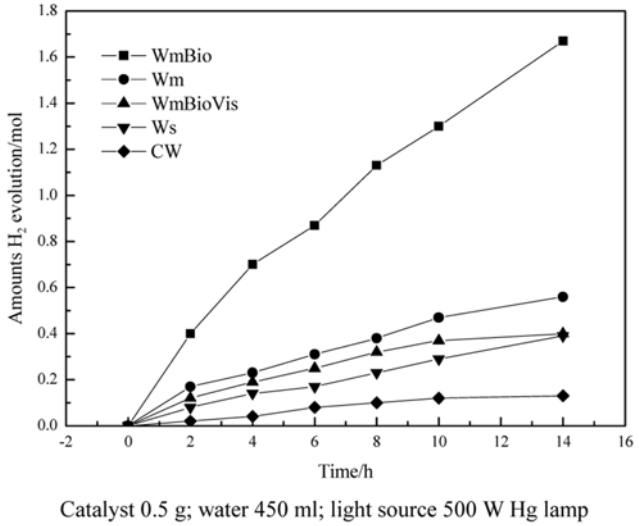

Fig. 7. Time course of photocatalytic decomposition of water over mesoporous Ws, Wm, $WO_3{\cdot}Bi_2O_3$, commerce WO_3.

($WO_3{\cdot}7.0$ wt% Bi_2O_3) and commercial WO_3 was made in medium pressure mercury lamp and visible light region. The result indicates that the photocatalytic activities of the mesoporous WO_3 samples prepared were higher in medium pressure mercury lamp and visible light region than commercial WO_3 (CW), for which the fact could be accounted that the mesoporous photocatalysts WO_3 had a larger specific surface area and higher crystallinity than commercial WO_3, and the remaining mesoporous framework. The materials involved had a zeolite-like mesoporous feature, which enhanced light absorption and multiple scattering, introduced continuous pore channels that facilitated the transfer of reactant molecules and electron-hole pair to surface, enhanced the transfer rate of charge on catalyst surface and inhabited the electron-hole pair recombination [17,18]. As a result, it was believed to be beneficial for increasing the photolytic reactivity and enhancing the photocatalytic degradation rate. However, the $WO_3{\cdot}Bi_2O_3$ exhibited the highest photocatalytic activity than the mesoporous WO_3 samples in Fig. 7, which has the largest band gap energies and during doping the Bi^{3+} ion into the wide band gap photocatalyst WO_3 favors inhabiting the electron-hole pair recombination and creating a visible absorption center and an active surface site, showing higher visible light responses [19,20] in photocatalysis. So, the evolution rate of H_2 for the sample $WO_3{\cdot}Bi_2O_3$ was about 167 $\mu mol{\cdot}h^{-1}$ under UV irradiation and about 40 $\mu mol{\cdot}h^{-1}$ under visible light irradiation. However, the photocatalytic activity under visible light irradiation was lower than UV-Vis irradiation, which may be due to the decrease in the total number of photons irradiated to WO_3 particles.

CONCLUSION

Mesoporous nano-crystalline WO_3 powders were successfully

synthesized by microwave heating under reflux and microwave extraction for removal of the surfactant species. The microwave extraction facilitated synthesizing uniform mesoporous structured materials. The mesoporous structured powder had the largest surface area and uniform mesoporous structure than materials synthesized by Soxhlet extracting and calcining; the UV-visible absorption was at wavelengths of about 500 nm. The photocatalytic reaction rate of mesoporous nano-crystalline of Bi-doped WO_3 was higher than commercial WO_3 photocatalysts in UV and visible light region. The results indicate that such a zeolite-like structural feature might have interesting bulk-chemistry applications, especially for heterogeneous photocatalysis.

ACKNOWLEDGEMENT

We gratefully acknowledge the financial support of the Natural Science Foundation of Education Office of Jiangxi, China (GJJ10506) and Provincial Natural Science Foundation of Jiangxi, China (2009GZH0002).

REFERENCES

1. V. Iliev, D. Tomova, L. Bilyarska, L. Prahov and L. Petrov, *J. Photochem. Photobiol. A: Chem.*, **159**, 281 (2003).
2. B. Warren Cross, P. Ivan Parkin and A. Shane O Neill, *Films Chem. Mater.*, **15**, 2786 (2003).
3. J. Luo and M. Hepel, *Electrochim. Acta*, **46**, 2913 (2001).
4. H. Kominami, J. I. Kato, S. Y. Murakami, Y. Ishii, M. Kohno, K. I. Yabutani, T. Yamamoto, Y. Kera, M. Inoue, T. Inui and B. Ohtani, *Catal. Today*, **84**, 186 (2003).
5. Gondal, et al., *Chem. Phys. Lett.*, **111**, 385 (2004).
6. A. Hameed, M. A. Gondal and Z. H. Yamani, *Catal. Commun.*, **715**, 5 (2004).
7. L. G. Teoha, J. S., W. H. Laia, I. M. Hunga and M. H. Hona, *J. Alloys Compounds*, **251**, 396 (2005).
8. S. Sallard, T. Brezesinski and M. S. Bernd, *J. Phys. Chem. C*, **7200**, 111 (2007).
9. X. Z. Cui, L. M. Guo, F. M. Cui, Q. J. He and J. Shi, *J. Phys. Chem. C*, **4134**, 113 (2009).
10. W. Wei, Y. Dai and B. B. Huang, *American Chem. Soc.*, **5658**, 113 (2009).
11. L. X. Zou, Q. Zhong and Q. C. Liu, *Transactions Mater. Heat Treat.*, **39**, 26 (2005).
12. L. X. Zou, Q. Zhong and Q. C. Liu, *Chem. Ind. Eng. Progress*, **1015**, 24 (2005).
13. L. Jiahe, D. Zhaoxiang, J. Xin, L. Fuli and L. Yadong, *Inorganic Chem.*, **234**, 41 (2002).
14. A. Antonaia, M. C. Santoro and G. Fameli, *Thin Solid Films*, **281**, 426 (2003).
15. J. Gabrusenoks, A. Veispals and A. Czarnowski, *Electrochim. Acta*, **2229**, 46 (2001).
16. S. Jan, H. G. S. Dmitry and J. Jianguang, *Chem. Mater.*, **5103**, 14 (2002).
17. T. Yoshiko, N. K. Junko and T. Tsuyoshi, *Chem. Mater.*, **1194**, 13 (2001).
18. C. J. Yu, X. C. Wang and X. Z. Fu, *Chem. Mater.*, **1523**, 16 (2004).
19. H. Hossam and P. Yaron, *J. Phys. Chem. B*, **2319**, 107 (2003).
20. S. Rodrigues, S. Uma, N. Igor, Martyanov and K. J. Klabunde, *J. Photochem. Photobiol. A: Chem.*, **51**, 165 (2004).